# Open Research Online

## Geometrically Tailored Skyrmions at Zero Magnetic Field in Multilayered Nanostructures

## Journal Item

For guidance on citations see FAQs.

## oro.open.ac.uk

# Geometrically Tailored Skyrmions at Zero Magnetic Field in Multilayered Nanostructures

Pin Ho,[1,2] Anthony K.C. Tan,[1,3] S. Goolaup,[1,2] A.L. Gonzalez Oyarce,[1,4] M. Raju,[3] L.S. Huang,[1,2] Anjan Soumyanarayanan,[1,2,3,*] and C. Panagopoulos[3,†]

[1] *Data Storage Institute, Agency for Science, Technology and Research (A*STAR), Singapore 138634, Singapore*

[2] *Institute of Materials Research and Engineering, Agency for Science, Technology and Research (A*STAR), Singapore 138634, Singapore*

[3] *Division of Physics and Applied Physics, School of Physical and Mathematical Sciences, Nanyang Technological University, Singapore 637371, Singapore*

[4] *Institute of High Performance Computing, Agency for Science, Technology and Research (A*STAR), Singapore 138632, Singapore*

Magnetic skyrmions are chiral spin structures recently observed at room temperature in multilayer films. Their topological stability will enable high scalability in confined geometries—a sought-after attribute for device applications. Despite numerous theoretical studies examining sub-100-nm Néel skyrmions in nanostructures, in practice their ambient stability and evolution with confinement and their magnetic parameters remain to be established. Here we present the zero-field stabilization of sub-100-nm room-temperature Néel-textured skyrmions confined in Ir/Fe($x$)/Co($y$)/Pt nanodots over a wide range of magnetic and geometric parameters. The zero-field skyrmion size, here as small as approximately 50 nm, can be tailored by a factor of 4 with variation of dot size and magnetic interactions. Crucially, skyrmions with differing thermodynamic stability exhibit an unexpected dichotomy in confinement phenomenologies. These results establish skyrmion phenomenology in multilayer nanostructures, and prompt the synergistic use of magnetic and geometric parameters to achieve desired properties in devices.

## I. INTRODUCTION

The topologically protected spin structure of skyrmions manifests itself in their emergent behavior as magnetic quasiparticles [1–3], with individual addressability, nucleation, and dynamics [4,5]. The discovery of room-temperature (RT) skyrmions in multilayer films [6–11]—material platforms of demonstrable technological relevance—has led to an explosion of interest in investigating their behavior in device-relevant configurations [12,13]. In particular, device proposals built upon their mobility in wires and manipulation in dots [5,14,15]. In the latter case, the topological stability of skyrmions [16] promises dot devices with nanometer scalability [4], ease of detection [4,17,18], and energy-efficient manipulation [4,15,19–21]. In particular, they could be used in magnetic-tunnel-junction configurations, with applications in memory [19,20], logic [13], and oscillators [14,22,23].

In this light, numerous theoretical studies have examined the formation and manipulation of single Néel skyrmions in ultrathin nanodots, and their scalability with geometric and magnetic parameters [5,24–28]. Meanwhile, experimental efforts on magnetic nanostructures have predominantly focused on Bloch skyrmions in low-temperature helimagnets [29,30], and chiral skyrmion bubbles (larger than 150 nm), the latter stabilized by long-range dipolar interactions [7,8,31,32]. However, technologically relevant Néel skyrmions, expected to possess sub-100-nm sizes in multilayers, have thus far been observed only at finite external magnetic fields [6,10], and are yet to exhibit confinement effects. Crucially, the ambient stabilization of confined skyrmions, the role of confinement in determining skyrmion properties, and its interplay with magnetic parameters all remain to be established.

Here we report the zero-field (ZF) stabilization of sub-100-nm RT skyrmions confined in nanodots of Ir/Fe($x$)/Co($y$)/Pt multilayer films (nominal layer thickness in angstroms in parentheses). High-resolution magnetic force microscopy (MFM) and micromagnetic simulations establish their existence over a wide range of magnetic and geometric parameters in our patterned dots. The ZF skyrmion size can be smoothly scaled by a factor of 4, down to as small as approximately 50 nm,

with variation of confinement and magnetic interactions. Crucially, confined skyrmions of differing thermodynamic stability unexpectedly exhibit contrasting phenomenologies. While metastable skyrmions conform to theoretical predictions, thermodynamically stable skyrmions form multiplets, with markedly different scaling characteristics with confinement. Our results prompt a revision of theoretical efforts on magnetic and geometric tailoring of confined skyrmions, and provide the cornerstone for engineering their properties for device applications.

## II. METHODS

### A. Film deposition

Multilayer stacks consisting of Ta(30)/Pt(100)/[Ir(10)/ **Fe($x$)/Co($y$)**/Pt(10)]$_{20}$/Pt(20) (nominal layer thicknesses in angstroms in parentheses) are deposited on thermally oxidized 100-mm Si wafers by dc magnetron sputtering at RT with use of a Chiron$^{\text{TM}}$ UHV system manufactured by Bestec GmbH. Five Fe($x$)/Co($y$) compositions are investigated here—Fe(2)/Co(6), Fe(2)/Co(5), Fe(3)/Co(6), Fe(4)/Co(6), and Fe(5)/Co(5), described henceforth by their Fe($x$)/Co($y$) composition—which enable the modulation of magnetic parameters (see Sec. S1 within the Supplemental Material [33]).

### B. Dot fabrication

Negative-resist Ma-N 2403 is spin coated on the multilayer films to form an approximately 300-nm-thick overlayer. Dots of diameter ($w$) 100–3000 nm are defined with use of an Elionix$^{\text{TM}}$ electron-beam-lithography tool. The patterns are transferred onto the multilayer films with use of an Intlvac$^{\text{TM}}$ ion-beam-etching system, with residual resist lifted off in an ultrasonic bath. Feature topography is imaged with use of a Veeco Dimension$^{\text{TM}}$ 3100 scanning probe microscope, and a JEOL$^{\text{TM}}$ JSM-7401 field-emission SEM. Cross-section SEM images [see, e.g., Fig. 1(a)] are obtained by our tilting the sample at 87°, with the sample mounted on a vertical holder.

Structural characterization of the dots shows an upright profile with relatively constant diameter vertically through the stacks for $w = 200$–500 nm (see Sec. S2 within the Supplemental Material [33]). For dots with $w \leq 150$ nm, a resist overlayer, due to incomplete lift-off, is observed in numerous cases [see, e.g., Fig. 4(b), i, $w = 150$ nm]. The resulting low yield for $w \leq 150$ nm precludes a direct comparison of magnetic phases across samples. While AFM images do show some skirting effects at the bottom boundary, the magnetic layers at the taper are too thin to contribute a detectable signal in MFM images.

### C. MFM measurements

MFM imaging is performed using a Veeco Dimension 3100 scanning probe microscope, with Co-alloy-coated SSS-MFMR$^{\text{TM}}$ tips. The sharp tip profile (diameter approximately 30 nm), its ultralow moment (approximately 80 emu/cm$^3$), and lift heights of 20–30 nm used during scanning provide high-resolution MFM images, while introducing minimal stray-field perturbations. Our earlier work established MFM as a reliable tool for imaging sub-100-nm skyrmions in multilayer film, producing $d_{\text{sk}}^m$ trends in excellent agreement with those obtained with x-ray-microscopy techniques [10]. While the lowest $d_{\text{sk}}^m$ values represent an overestimate due to implicit convolution with the approximately 30-nm MFM probe, this effect can be straightforwardly quantified [10,34]. In this work, the dots are imaged after *ex situ* negative out-of-plane (OP) saturation, followed by the application of *in situ* OP fields ranging from 0 to 200 mT. The magnetization orientation of the skyrmion core is twofold degenerate—its MFM signal is determined by the relative directions of the tip and sample saturation. Repeated MFM scans are acquired to ensure consistency and reproducibility of results. Twelve dots are imaged for each $w$ and Fe/Co composition to mitigate variability in deposition and fabrication processes.
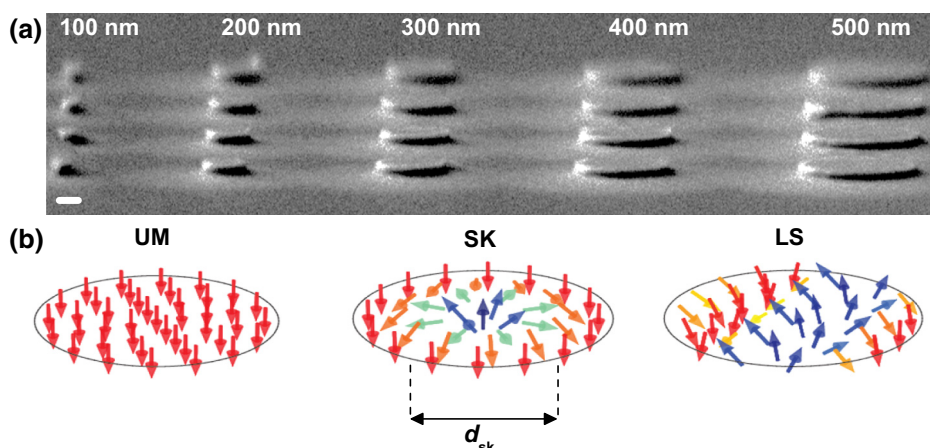


FIG. 1. Confined magnetic states in nanodots. (a) Scanning-electron-microscope image (scale bar 100 nm) of an [Ir/Fe/Co/Pt]$_{20}$-dot array with diameter $w$ ranging from 100 to 500 nm. (b) Spin textures corresponding to the three distinct states expected in multilayer nanodots: uniform magnetization (UM), Néel skyrmion (SK; size $d_{\text{sk}}$), and labyrinthine stripes (LS).

### D. Micromagnetic simulations

Micromagnetic simulations are performed with MUMAX³-based simulation software [35]. The dot is defined with a cylindrical geometry, in line with experimentally fabricated structures. The mesh cell size used has lateral dimensions of $(2–4) \times (2–4)$ nm², while the vertical size $t_{FM}$ is set to match the Fe/Co magnetic layer thickness of each sample [e.g., $t_{FM} = 0.8$ nm for Fe(2)/Co(6)]. The adjacent magnetic layers (Fe and Co) are simulated as a single cell to mimic the experimentally observed persistence of skyrmion textures across both layers [10]. An approximately 2-nm spacer layer is introduced between magnetic layers (for Ir and Pt), with the spacer thickness approximated to be the nearest multiple of $t_{FM}$. The results shown correspond to simulations of 20 stack repeats, consistent with the experimental multilayer film. Single-stack simulations are performed for illustrative comparison.

The magnetic parameters used are consistent with our film-level results on [Ir/Co($x$)/Fe($y$)/Pt]$_{20}$ stacks [10] (see Sec. S1 within the Supplemental Material [33]), and the Gilbert damping parameter $\alpha$ is set to 0.1. A single (or multiple) skyrmion configuration is initialized in the dot,

and the magnetization is allowed to relax over a timescale of approximately 2–10 ns to simulate the ZF configuration for each set of parameters (see Sec. S4 within the Supplemental Material [33]). MFM images are generated from the two-dimensional magnetization profile with use of the MUMAX³ built-in MFM function [35], with a tip height of 20 nm and a dipole size of 30 nm.

## III. CONFINED STATES IN MULTILAYERS

The ground-state configuration of a magnetic multilayer nanostructure is governed by the collective influence of magnetic interactions. The exchange interaction, characterized by the stiffness ($A$), aligns neighboring spins parallel and favors a uniformly magnetized (UM) state [Fig. 1(b)], with orientation determined by the effective (OP) anisotropy, $K_{eff}$. In contrast, the interfacial Dzyaloshinskii-Moriya interaction ($D$) prefers a winding spin arrangement, leading to a labyrinthine-stripe (LS) state [Fig. 1(b)] [36]. The competition between $D$, $A$, and $K_{eff}$ can form Néel-textured skyrmions [SKs; Fig. 1(b)]
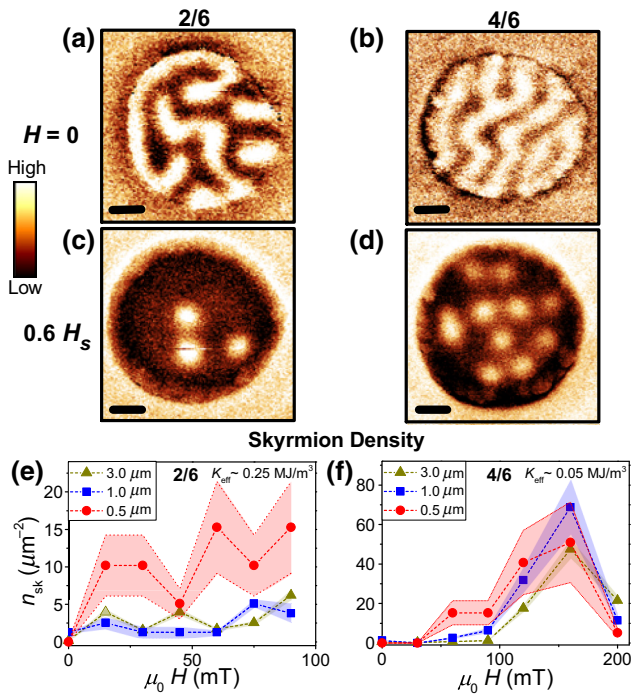


FIG. 2.   Confinement effects in submicron dots. (a)–(d) MFM images (scale bar 100 nm) of dots with $w = 500$ nm after negative saturation for (a),(c) Fe(2)/Co(6) stacks and (b),(d) Fe(4)/Co(6) stacks. At $H = 0$, (a),(b) show LS states. At $H \simeq 0.6\,H_S$ (out-of-plane saturation field) (c),(d) show SK states in isolated (c) and lattice (d) configurations. (e),(f) Measured skyrmion density $n_{sk}$ as a function of $H$ for dots with differing $w$ for (e) Fe(2)/Co(6) and (f) Fe(4)/Co(6). Shaded regions represent error bars.
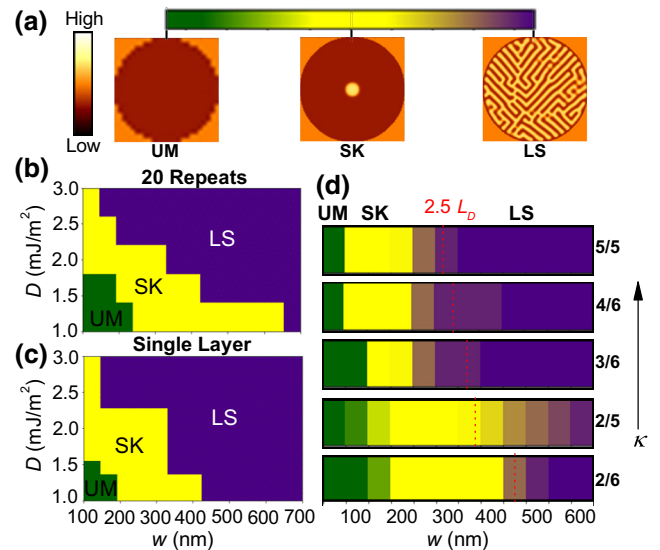


FIG. 3.   Simulated evolution of ZF magnetic states. Micromagnetic simulations of the ZF phase diagram for [Ir/Fe($x$)/Co($y$)/Pt]$_{20}$ dots. (a) The magnetic textures obtained are identified as UM (green), SK (yellow), or LS (blue). Phase diagrams with parameters for Fe(2)/Co(6) for (b) 20 repeats and (c) a single layer, with $D$ and $w$ varied over a range of likely values. The SK state is expected over a broad, intermediate set of parameters. (d) Expected evolution of magnetic states in dots with $w$ ranging from 50 to 600 nm across the five samples [shown with increasing $\kappa$ in Fig. 4(a); see Sec. S1 within the Supplemental Material [33]]. A weighted-average method is adopted to estimate the expected magnetic state for each $w$ (see Sec. S4 within the Supplemental Material [33]).
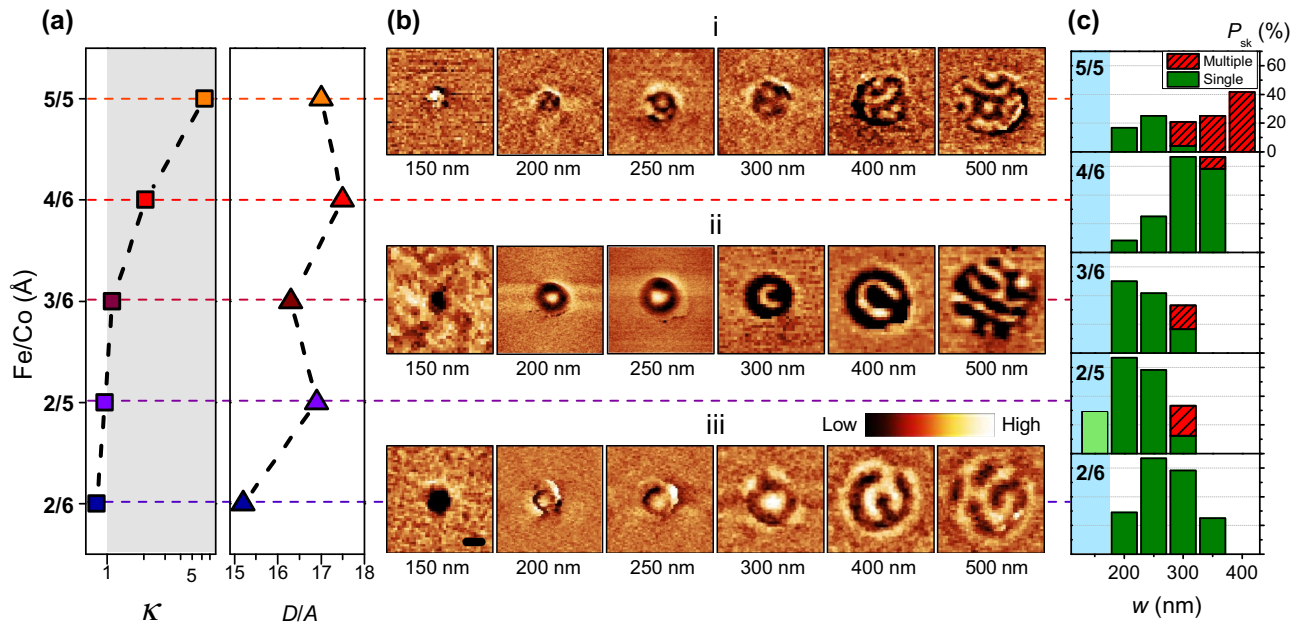
FIG. 4. Imaging confined ZF skyrmions. (a) Variation of $\kappa$ and $D/A$ across the samples studied. (b) MFM images at ZF (scale bar 100 nm) showing the magnetic states in dots with $w$ ranging from 150–500 nm for Fe(2)/Co(6), Fe(3)/Co(6), and Fe(5)/Co(5) respectively. The images, in several cases, show ZF skyrmions at intermediate $w$, with UM and LS phases for smaller and larger $w$ respectively. (c) Empirical ZF skyrmion nucleation probability, $P_{sk}$ (averaged over 12 nominally identical dots), as a function of $w$ for all five samples. The shaded blue region ($w < 200$ nm) indicates a low yield from the patterning process. Both single (green bars) and multiple (red bars) skyrmion configurations are observed.

[4], thermodynamically stable entities for material parameter $\kappa > 1$, where $\kappa = \pi D/4\sqrt{AK_{eff}}$ [1,3,10]. Moreover, the presence of interlayer dipolar coupling in multilayer stacks [28,37,38] and long-range intralayer dipolar interactions [8] can also play a role—the latter being key to stabilizing larger (>200 nm) skyrmion bubbles [7–9,28,32]. Notably, confined geometries can shape the ground state [8,24,29,30,37,39], potentially favoring ZF stabilization of skyrmions [5,24].

The stability and size of confined skyrmions would be markedly influenced by magnetic interactions and geometric parameters [24,28,37]. Multilayer [Ir(10)/Fe(x)/Co(y)/Pt(10)]$_{20}$ stacks (layer thicknesses in angstroms in parentheses), wherein magnetic interactions can be tailored by the Fe(x)/Co(y) composition, are a suitable platform for establishing confined Néel-textured skyrmion phenomenology [34]. We investigate RT skyrmions in dots ($w = 100$–3000 nm) patterned from these stacks [see, e.g., Fig. 1(a)]. On establishing consistency between magnetic textures in dots with $w \geq 1000$ nm and film-level results (see Sec. S3 within the Supplemental Material [33]), we examine the effect of confinement as $w$ is reduced to 500 nm. For the representative sample Fe(2)/Co(6), we find a LS state at ZF [Fig. 2(a)], which transforms to sub-100-nm skyrmions at finite OP fields [$H$; Fig. 2(c)]. Notably, the skyrmion density, $n_{sk}$, is consistently higher in 500-nm dots, by a factor of 3, as compared with larger dots

and films [Fig. 2(e)], and this is attributed to the reduction in magnetostatic energy with smaller $w$ [7,8]. Meanwhile, for dots with lower $K_{eff}$ [Figs. 2(b), 2(d), and 2(f)], $n_{sk}(H)$ is consistent across $w$, and is approximately 5–10 times greater than for Fe(2)/Co(6). Indeed, $n_{sk}$ is known to increase with reducing $K_{eff}$ as the energy barrier for domain nucleation is lowered. Importantly, the constancy of $n_{sk}$ with $w$ for Fe(4)/Co(6)—which already hosts a dense skyrmion lattice—offers an orthogonal tuning parameter. This suggests that use of the synergy between magnetic tuning and confinement is a promising route for tailoring ZF skyrmions.

## IV. CONFINED ZERO-FIELD SKYRMIONS

Next we perform a comprehensive set of multilayer micromagnetic simulations to map the evolution of magnetic states for dots with $w < 500$ nm. The relaxed magnetic state at ZF, following the introduction of a skyrmion, is examined over a range of parameters to determine the magnetic phase diagram (Fig. 3; see Sec. S4 within the Supplemental Material [33]) [5,7]. While the LS phase dominates at large $w$, the reduction in magnetostatic energy for intermediate $w$ shrinks the stable domain wall size, and instead favors the formation of a SK phase [24]. As $w$ is reduced further (below approximately 100 nm), the exchange energy eventually dominates, leading to the UM
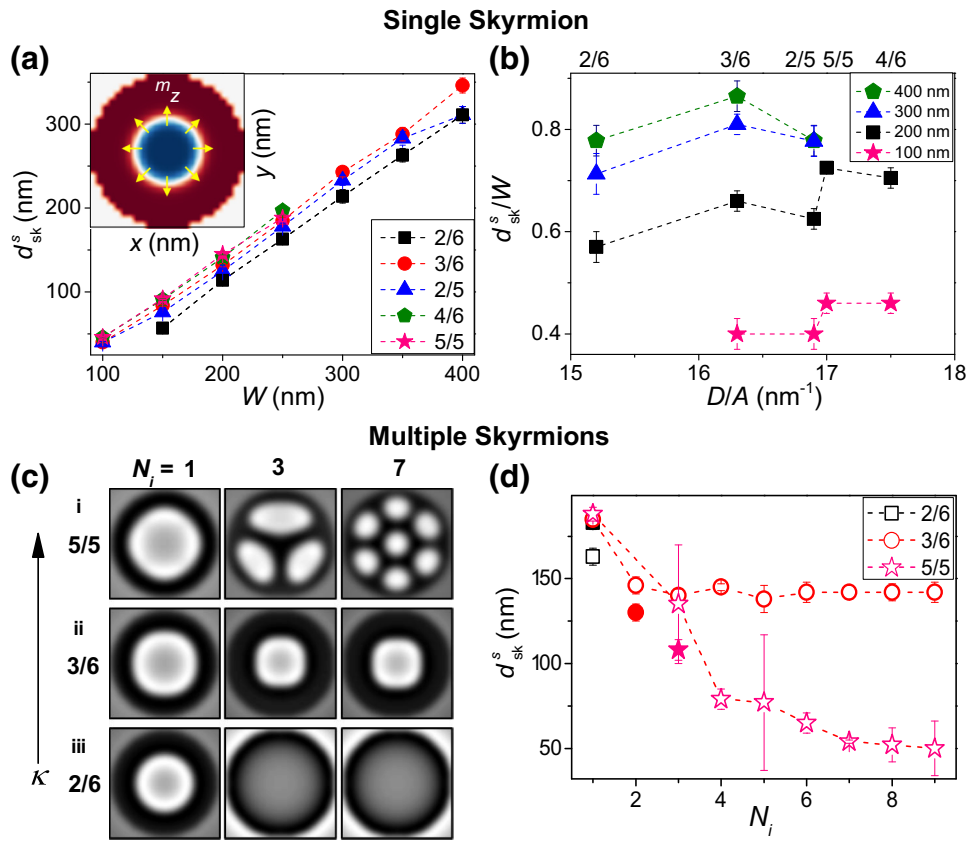
FIG. 5. Simulated skyrmion size variation. (a) $d_{sk}^s$ trend for a single skyrmion initialized and relaxed in a dot, with variation of $w$ across samples. The inset shows magnetization (color scale, $m_z$; arrows, IP texture) of a Néel skyrmion in the dot. (b) Modulation of $d_{sk}^s/w$ [values from (a)] with $D/A$ across samples. (c),(d) Simulated initialization of different numbers ($N_i$) of skyrmions in a dot with $w = 250$ nm for Fe(2)/Co(6), Fe(3)/Co(6), and Fe(5)/Co(5) of increasing $\kappa$. (c) Simulated MFM images for three $N_i$ values, showing differing numbers of stabilized skyrmions. (d) Variation of $d_{sk}^s$ with $N_i$ (open symbols) for $N_i > 1$, with qualitatively different trends in comparison with $N_i = 1$. Solid symbols show measured $d_{sk}^m$ values from experiments.

phase. The interplay between confinement and magnetic parameters determines the window for SK stability in dots, which is explored here.

First, a comparison of the phase diagrams for the Fe(2)/Co(6) multilayer [Fig. 3(b)] and the corresponding single layer [Fig. 3(c)] shows the SK phase persisting over a much larger $w$ range in the multilayer. The additional presence of interlayer dipolar coupling, introduced by multilayer stacking, is key to this increased SK stability [28,38]. Next, an inspection of the confined magnetic states across samples [Fig. 3(d), optimal parameters] suggests that ZF skyrmions may be observed for $w \lesssim 2.5 L_D$ ($L_D$ is the film-level domain periodicity), and the stability in smaller dots could be enhanced with increasing $\kappa$.

We now turn to MFM images of ZF magnetic textures for dots with $w < 500$ nm, shown for three illustrative samples in Fig. 4(b) (corresponding data for 2/5 and 4/6 can be found in Sec. S3 within the Supplemental Material [33]). Consistent with simulations [Fig. 3(d)], reducing $w$ [from 500 to 150 nm: Fig. 4(b), right to left] results in a gradual transition from the LS phase to the SK phase, and eventually to the UM phase. Crucially, sub-100-nm skyrmions are stabilized at ZF, *prima facie* by confinement effects, across all Ir/Fe($x$)/Co($y$)/Pt compositions. In some cases, however, nominally identical dots are found

to exhibit different ZF states, likely due to the granularity of sputtered films [32,40,41], or fabrication-process variations (see Sec. II and Sec. S2 within the Supplemental Material [33]). This variability is mitigated by our determining the statistically averaged behavior of 12 dots for each $w$ across samples. The evolution of ZF skyrmion-state probability, $P_{sk}$, is examined here.

Histogram plots of skyrmion nucleation probability, $P_{sk}(w)$ [Fig. 4(c)], evidence a stable SK phase over a range of magnetic [Fig. 4(a)] and geometric parameters. In line with simulations (Fig. 3), the increased skyrmion stability in multilayers underscores the vital role of interlayer dipolar interactions. Next, while the peak $P_{sk}$ appears to shift to lower $w$ with $\kappa$ for $\kappa \lesssim 1$, this trend, expected from simulations, does not persist for $\kappa > 1$. For $w < 200$ nm [Fig. 4(c), shaded region], the low yield in our patterning process precludes a statistically meaningful comparison across $\kappa$ (see Sec. II).

More surprising is the persistence of the SK phase for $\kappa > 1$ at larger $w$, particularly the observation of multiskyrmion configurations [see, e.g., Fig. 4(b), i, 300 nm; Fig. 4(c), red]. While thermodynamically stable skyrmions ($\kappa > 1$) form ordered lattices at finite fields [1,2,4,10,29], the presence of multiskyrmion configurations suggests a strong interplay of magnetic and confinement effects not considered in previous simulations. Indeed, when

simulations are repeated with the initialized skyrmion number, $N_i > 1$ [Fig. 5(c); see Sec. S4 within the Supplemental Material [33] ] [7,39], multiskyrmion states are found for dots with $\kappa > 1$ [Fig. 5(c), i]. In contrast, multiskyrmion states are consistently absent in dots with $\kappa < 1$ both in experiments [Fig. 4(b), iii] and in simulations [Fig. 5(c), iii], and only single skyrmions are formed across $w$.

## V. VARIATION OF SKYRMION SIZE

A visible modulation in the experimentally measured skyrmion size, $d_{sk}^m$ across magnetic (vertical) and geometric (horizontal) parameters is seen in Fig. 4(b). For comparison, Fig. 5(a) summarizes the simulated $d_{sk}^s$ trends for $N_i = 1$, showing a near-identical $w$ dependence across samples. This corresponds to a weak dependence of the normalized size $d_{sk}^s/w$ on magnetic parameters [e.g., $D/A$; Fig. 5(b)], consistent with recent multilayer simulations by other groups [28,37]. However, such insensitivity of $d_{sk}^s$ to magnetic parameters is in stark contrast with our MFM data [Fig. 4(b)]. A reconciliation with measured $d_{sk}$ trends would require our accounting for multiskyrmion stability for $\kappa \gtrsim 1$.

The relaxed magnetic configuration for $N_i > 1$ simulations [Figs. 5(c) and 5(d) for $w = 250$ nm] shows a marked transformation with variation of $\kappa$, in line with experimental trends [Fig. 4(b)]. First, for $\kappa < 1$ [Fig. 5(c), iii], only single skyrmions can be stabilized, and only with $N_i = 1$; $N_i > 1$ simulations relax to a UM state. Next, for $\kappa \sim 1$ [Fig. 5(c), ii], $N_i > 1$ simulations relax to a single skyrmion, albeit with reduced $d_{sk}^s$. Finally, for $\kappa > 1$ [Fig. 5(c), i], multiskyrmion configurations are formed for $N_i > 1$, while $d_{sk}^s$ reduces and plateaus for larger

$N_i$. Importantly, these $d_{sk}^s$ values [Fig. 5(d), open symbols] agree qualitatively with measured $d_{sk}^m$ trends [Fig. 5(d); filled symbols] for appropriate $N_i$. We suggest that the inclusion of magnetic granularity [40,41] and interlayer coupling [32,38] in a future simulation model could improve the quantitative agreement of $d_{sk}^s$ with experimental values.

Figure 6(a) summarizes the measured ZF $d_{sk}^m$ trends, showing an overall factor-of-4 reduction—from approximately 200 nm to approximately 50 nm. Notably, $d_{sk}^m$ is monotonically reduced with increased confinement for all samples, with up to 2.5 times reduction for Fe(2)/Co(6). Similarly, for a given dot size, $d_{sk}^m$ varies by up to 2.5 times across samples. Most interesting in Fig. 6(a) is the marked disparity in the $w$ dependence of $d_{sk}^m$. The confinement gradient, defined as $\delta d_{sk}^m/\delta w$, reduces by 4 times across samples. This observation, while incongruous with $N_i = 1$ simulations for $\kappa > 1$ [Fig. 5(a)] [5,24,37], is consistent with the behavior of multiskyrmion states [Fig. 5(d)].

Finally we examine the evolution of $d_{sk}^m$ with $D/A$ [Fig. 6(b)] and $H$ [Fig. 6(c)] in the context of extensive predictions of these trends [5,6,24,27,28,37]. Figure 6(b) shows that the normalized size, $d_{sk}^m/w$, reduces monotonically with increasing $D/A$, with a sharp jump at $\kappa \sim 1$. The sudden reduction (up to 2 times) in $d_{sk}^m/w$ across all $w$ indicates a fundamental change in confined-skyrmion behavior around $\kappa \simeq 1$, consistent with recent predictions [28]. Figure 6(c) shows the expected reduction in $d_{sk}^m$ with increasing $H$ across samples. However, the 20–30% reduction (for 0–30 mT) seen here is considerably less than the 2–3 times reduction reported for larger confined skyrmions with similar fields [7,8,32]. Furthermore, the ZF trend of $d_{sk}^m(w)$ is found to persist
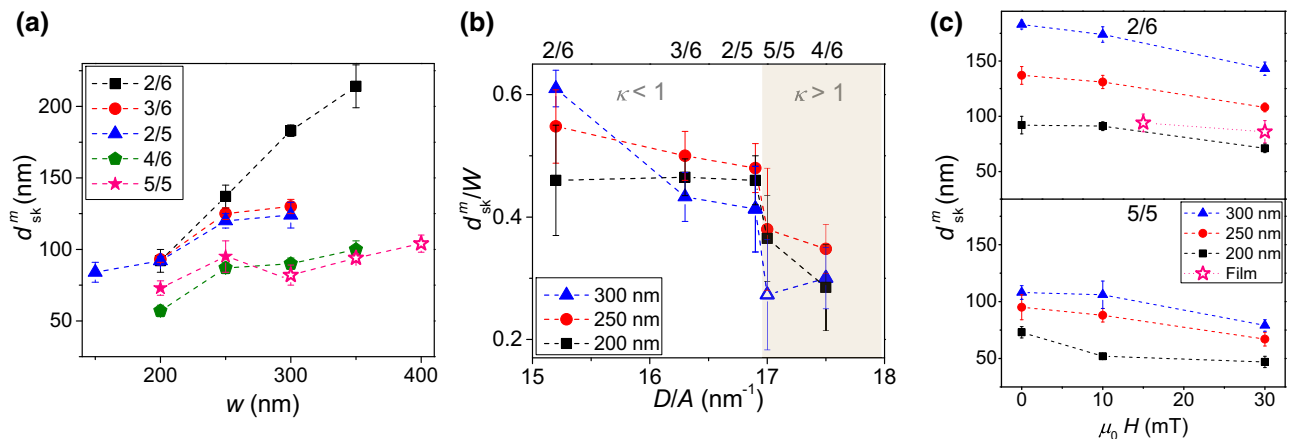


FIG. 6. Measured variation of skyrmion size. (a) Summary of measured $d_{sk}^m$ values at ZF (isotropic Gaussian fits to MFM data) for all samples across dot sizes. Visible trends in $d_{sk}^m$ magnitude and the extent of its $w$ dependence are observed across samples. Open symbols are derived from multiskyrmion configurations. (b) The ratio $d_{sk}^m/w$ for several values of $w$ versus $D/A$ [see Fig. 5(c)]. (c) Field dependence of $d_{sk}^m$ for two representative samples—Fe(2)/Co(6) (film-level results included for comparison) and Fe(5)/Co(5)—for several values of $w$.

at finite fields—smaller dots consistently host smaller skyrmions—in contrast with prior reports [6]. This highlights the demonstrable robustness of confinement effects in Ir/Fe/Co/Pt dots.

## VI. CONCLUSION

We present a comprehensive picture of confinement-induced skyrmion formation and evolution at ZF in Ir/Fe($x$)/Co($y$)/Pt dots. Sub-100-nm skyrmions are stabilized at ZF over a wide range of magnetic and geometric parameters by intrinsic, interlayer, and confinement-induced magnetic interactions. The size of these skyrmions, here as small as approximately 50 nm, varies with magnetic and geometric parameters by up to approximately 2.5 times in either case. Finally, the ZF stability of multiskyrmion configurations for $\kappa \gtrsim 1$ and the stark contrast in size evolution across $\kappa = 1$ suggest a strong synergy of thermodynamic and confinement effects. These results provide a platform for harnessing the properties of nanoscale skyrmions in confined geometries.

First, the sub-100-nm Néel skyrmions at ZF reported here show markedly different physical characteristics from confined skyrmion bubbles [7,8,32]. This indicates that despite their nominally identical topological characteristics [12,13], exploration of the stability [28], structure [32], and mobility [40] of these spin textures could require independent lines of investigation. Our comprehensive investigation of confined Néel skyrmions offers a firm foundation tailor-made for such efforts. Second, the manifestly distinct trends in skyrmion configuration and size with variation of $\kappa$ go beyond existing predictions [5,24, 27,28]. While recent studies have incorporated the effects of granularity [32,41], interlayer coupling [6], and dipolar interactions [28,37], we posit that future studies of confined skyrmions would benefit from harnessing their differing behavior with thermodynamic stability. Finally, the elastic tuning of skyrmion size with confinement opens up the exciting possibility of designer magnetic lattices with topological properties—with the potential to engineer frustration, criticality, and topology under ambient conditions [42].

Crucially, the realization of sub-100-nm ZF skyrmions in a device-relevant geometry prompts their immediate use along technological lines, especially within perpendicular magnetic-tunnel-junction devices. First, the demonstrable modulation of their stability and size with magnetic interactions and confinement enables mechanistic investigations of skyrmion creation [4], detection [17,18], and dynamics [5] in ambient, device-ready conditions. Next, their sub-100-nm size and ZF stability over a wide range would make possible energy-efficient microwave detectors [14], oscillators [23], spin valves [22], and magnonic crystals [43]. Finally, their topological stability and malleability with confinement are particularly suited

for highly scalable realizations of random access memory and synaptic computing [44].

[1] A. N. Bogdanov and U. K. Rößler, Chiral Symmetry Breaking in Magnetic Thin Films and Multilayers, Phys. Rev. Lett. **87,** 037203 (2001).

[2] Naoto Nagaosa and Yoshinori Tokura, Topological properties and dynamics of magnetic skyrmions, Nat. Nanotechnol. **8,** 899 (2013).

[3] Anjan Soumyanarayanan, Nicolas Reyren, Albert Fert, and Christos Panagopoulos, Emergent phenomena induced by spin-orbit coupling at surfaces and interfaces, Nature **539,** 509 (2016).

[4] Niklas Romming, Christian Hanneken, Matthias Menzel, Jessica E. Bickel, Boris Wolter, and Kirsten von Bergmann, Writing and deleting single magnetic skyrmions, Science **341,** 636 (2013).

[5] J. Sampaio, V. Cros, S. Rohart, A. Thiaville, and A. Fert, Nucleation, stability and current-induced motion of isolated magnetic skyrmions in nanostructures, Nat. Nanotechnol. **8,** 839 (2013).

[6] C. Moreau-Luchaire, C. Moutafis, N. Reyren, J. Sampaio, C. A. F. Vaz, N. Van Horne, K. Bouzehouane, K. Garcia, C. Deranlot, P. Warnicke, P. Wohlhüter, J.-M. George, M. Weigand, J. Raabe, V. Cros, and A. Fert, Additive interfacial chiral interaction in multilayers for stabilization of small individual skyrmions at room temperature, Nat. Nanotechnol. **11,** 444 (2016).

[7] Seonghoon Woo, Kai Litzius, Benjamin Krüger, Miyoung Im, Lucas Caretta, Kornel Richter, Maxwell Mann, Andrea Krone, Robert M. Reeve, Markus Weigand, Parnika Agrawal, Ivan Lemesh, Mohamad Assaad Mawass, Peter

Fischer, Mathias Kläui, and Geoffrey S. D. Beach, Observation of room-temperaturemagnetic skyrmions and their current-driven dynamics in ultrathin metallic ferromagnets, Nat. Mater. **15,** 501 (2016).

[8] Olivier Boulle, Jan Vogel, Hongxin Yang, Stefania Pizzini, Dayane de Souza Chaves, Andrea Locatelli, Tevfik Onur Mentes, Alessandro Sala, Liliana D. Buda-Prejbeanu, Olivier Klein, Mohamed Belmeguenai, Yves Roussigné, Andrey Stashkevich, Salim Mourad Chérif, Lucia Aballe, Michael Foerster, Mairbek Chshiev, Stéphane Auffret, Ioan Mihai Miron, and Gilles Gaudin, Room-temperature chiral magnetic skyrmions in ultrathin magnetic nanostructures, Nat. Nanotechnol. **11,** 449 (2016).

[9] W. Jiang, P. Upadhyaya, W. Zhang, G. Yu, M. B. Jungfleisch, F. Y. Fradin, J. E. Pearson, Y. Tserkovnyak, K. L. Wang, O. Heinonen, S. G. E. te Velthuis, and A. Hoffmann, Blowing magnetic skyrmion bubbles, Science **349,** 283 (2015).

[10] Anjan Soumyanarayanan, M. Raju, A. L. GonzalezOyarce, Anthony K. C. Tan, Mi-Young Im, A. P. Petrovic, Pin Ho, K. H. Khoo, M. Tran, C. K. Gan, F. Ernult, and C. Panagopoulos, Tunable room temperature magnetic skyrmions in Ir/Fe/Co/Pt multilayers, Nat. Mater. **16,** 898 (2017).

[11] Wanjun Jiang, Gong Chen, Kai Liu, Jiadong Zang, Suzanne G. E. te Velthuis, and Axel Hoffmann, Skyrmions in magnetic multilayers, Phys. Rep. **704,** 1 (2017).

[12] Giovanni Finocchio, Felix Büttner, Riccardo Tomasello, Mario Carpentieri, and Mathias Kläui, Magnetic skyrmions: From fundamental to applications, J. Phys. D: Appl. Phys. **49,** 423001 (2016).

[13] Albert Fert, Nicolas Reyren, and Vincent Cros, Magnetic skyrmions: Advances in physics and potential applications, Nat. Rev. Mater. **2,** 17031 (2017).

[14] G. Finocchio, M. Ricci, R. Tomasello, A. Giordano, M. Lanuzza, V. Puliafito, P. Burrascano, B. Azzerboni, and M. Carpentieri, Skyrmion based microwave detectors and harvesting, Appl. Phys. Lett. **107,** 262401 (2015).

[15] Bin Zhang, Weiwei Wang, Marijan Beg, Hans Fangohr, and Wolfgang Kuch, Microwave-induced dynamic switching of magnetic skyrmion cores in nanodots, Appl. Phys. Lett. **106,** 102401 (2015).

[16] J. Hagemeister, N. Romming, K. von Bergmann, E. Y. Vedmedenko, and R. Wiesendanger, Stability of single skyrmionic bits, Nat. Commun. **6,** 8455 (2015).

[17] Christian Hanneken, Fabian Otte, André Kubetzka, Bertrand Dupé, Niklas Romming, Kirsten von Bergmann, Roland Wiesendanger, and Stefan Heinze, Electrical detection of magnetic skyrmions by tunnelling non-collinear magnetoresistance, Nat. Nanotechnol. **10,** 1039 (2015).

[18] Riccardo Tomasello, Marco Ricci, Pietro Burrascano, Vito Puliafito, Mario Carpentieri, and Giovanni Finocchio, Electrical detection of single magnetic skyrmion at room temperature, AIP Adv. **7,** 056022 (2017).

[19] Y. Nakatani, M. Hayashi, S. Kanai, S. Fukami, and H. Ohno, Electric field control of skyrmions in magnetic nanodisks, Appl. Phys. Lett. **108,** 152403 (2016).

[20] Dhritiman Bhattacharya and Jayasimha Atulasimha, Skyrmion mediated voltage controlled switching of ferromagnets for reliable and energy efficient 2-terminal memory, ACS Appl. Mater. Interfaces **10,** 17455 (2017).

[21] S. Seki, X. Z. Yu, S. Ishiwata, and Yoshinori Tokura, Observation of skyrmions in a multiferroic material, Science **336,** 198 (2012).

[22] Y. Zhou, E. Iacocca, A. A. Awad, R. K. Dumas, F. C. Zhang, H. B. Braun, and J. Åkerman, Dynamically stabilized magnetic skyrmions, Nat. Commun. **6,** 8193 (2015).

[23] F. Garcia-Sanchez, J. Sampaio, N. Reyren, V. Cros, and J.-V. Kim, A skyrmion-based spin-torque nano-oscillator, New J. Phys. **18,** 075011 (2016).

[24] S. Rohart and A. Thiaville, Skyrmion confinement in ultrathin film nanostructures in the presence of Dzyaloshinskii-Moriya interaction, Phys. Rev. B **88,** 184422 (2013).

[25] Konstantin Y. Guslienko, Skyrmion state stability in magnetic nanodots with perpendicular anisotropy, IEEE Magn. Lett. **6,** 4000104 (2015).

[26] A. G. Kolesnikov, A. S. Samardak, M. E. Stebliy, A. V. Ognev, L. A. Chebotkevich, A. V. Sadovnikov, S. A. Nikitov, Yong Jin Kim, In Ho Cha, and Young Keun Kim, Spontaneous nucleation and topological stabilization of skyrmions in magnetic nanodisks with the interfacial Dzyaloshinskii-Moriya interaction, J. Magn. Magn. Mater. **429,** 221 (2017).

[27] R. Tomasello, K. Y. Guslienko, M. Ricci, A. Giordano, J. Barker, M. Carpentieri, O. Chubykalo-Fesenko, and G. Finocchio, Origin of temperature and field dependence of magnetic skyrmion size in ultrathin nanodots, Phys. Rev. B **97,** 060402 (2018).

[28] M. Zelent, J. Tóbik, M. Krawczyk, K. Y. Guslienko, and M. Mruczkiewicz, Bi-stability of magnetic skyrmions in ultrathin multilayer nanodots induced by magnetostatic interaction, Phys. Status Solidi Rapid Res. Lett. **11,** 1770350 (2017).

[29] Xuebing Zhao, Chiming Jin, Chao Wang, Haifeng Du, Jiadong Zang, Mingliang Tian, Renchao Che, and Yuheng Zhang, Direct imaging of magnetic field-driven transitions of skyrmion cluster states in FeGe nanodisks, Proc. Natl. Acad. Sci. U. S. A. **113,** 4918 (2016).

[30] Fengshan Zheng, Hang Li, Shasha Wang, Dongsheng Song, Chiming Jin, Wenshen Wei, Mingliang Tian, Yuheng Zhang, Haifeng Du, and Rafal E. Dunin-Borkowski, Direct Imaging of a Zero-Field Target Skyrmion and Its Polarity Switch in a Chiral Magnetic Nanodisk, Phys. Rev. Lett. **119,** 197205 (2017).

[31] Dustin A. Gilbert, Brian B. Maranville, Andrew L. Balk, Brian J. Kirby, Peter Fischer, Daniel T. Pierce, John Unguris, Julie A. Borchers, and Kai Liu, Realization of ground-state artificial skyrmion lattices at room temperature, Nat. Commun. **6,** 9462 (2015).

[32] K. Zeissler, M. Mruczkiewicz, S. Finizio, J. Raabe, P. M. Shepley, A. V. Sadovnikov, S. A. Nikitov, K. Fallon, S. McFadzean, S. McVitie, T. A. Moore, G. Burnell, and C. H. Marrows, Pinning and hysteresis in the field dependent diameter evolution of skyrmions in Pt/Co/Ir superlattice stacks, Sci. Rep. **7,** 15125 (2017).

[33] See Supplemental Material at http://link.aps.org/supplemental/10.1103/PhysRevApplied.11.024064 for details of the experiments and simulations.

[34] A. Yagil, A. Almoalem, Anjan Soumyanarayanan, Anthony K. C. Tan, M. Raju, C. Panagopoulos, and O. M. Auslaender, Stray field signatures of Neel textured skyrmions in

Ir/Fe/Co/Pt multilayer films, Appl. Phys. Lett. **112**, 192403 (2017).

[35] Arne Vansteenkiste, Jonathan Leliaert, Mykola Dvornik, Mathias Helsen, Felipe Garcia-Sanchez, and Bartel Van Waeyenberge, The design and verification of MuMax3, AIP Adv. **4**, 107133 (2014).

[36] M. Heide, G. Bihlmayer, and S. Blügel, Dzyaloshinskii-Moriya interaction accounting for the orientation of magnetic domains in ultrathin films: Fe/W(110), Phys. Rev. B **78**, 140403 (2008).

[37] Nicolás Vidal-Silva, Alejandro Riveros, and Juan Escrig, Stability of Neel skyrmions in ultra-thin nanodots considering Dzyaloshinskii-Moriya and dipolar interactions, J. Magn. Magn. Mater. **443**, 116 (2017).

[38] Javier F. Pulecio, Aleš Hrabec, Katharina Zeissler, Yimei Zhu, and Christopher H. Marrows, Phase Transitions of Chiral Spin Textures via Dipolar Coupling in Multilayered Films with Interfacial DMI, arXiv:1611.00209 [cond-mat.mtrl-sci] (2016).

[39] Marijan Beg, Rebecca Carey, Weiwei Wang, David Cortés-Ortuõ, Mark Vousden, Marc-Antonio Bisotti, Maximilian Albert, Dmitri Chernyshenko, Ondrej Hovorka, Robert L. Stamps, and Hans Fangohr, Ground state search, hysteretic behaviour, and reversal mechanism of skyrmionic textures in confined helimagnetic nanostructures, Sci. Rep. **5**, 17137 (2015).

[40] William Legrand, Davide Maccariello, Nicolas Reyren, Karin Garcia, Christoforos Moutafis, Constance Moreau-Luchaire, Sophie Collin, Karim Bouzehouane, Vincent Cros, and Albert Fert, Room-temperature current-induced generation and motion of sub-100 nm skyrmions, Nano Lett. **17**, 2703 (2017).

[41] Roméo Juge, Soong-Geun Je, Dayane de Souza Chaves, Stefania Pizzini, Liliana D. Buda-Prejbeanu, Lucia Aballe, Michael Foerster, Andrea Locatelli, Tevfik Onur Mentes, Alessandro Sala, Francesco Maccherozzi, Sarnjeet S. Dhesi, Stéphane Auffret, Gilles Gaudin, Jan Vogel, and Olivier Boulle, Magnetic skyrmions in confined geometries: Effect of the magnetic field and the disorder, J. Magn. Magn. Mater. **455**, 3 (2018).

[42] Cristiano Nisoli, Roderich Moessner, and Peter Schiffer, Colloquium: Artificial spin ice: Designing and imaging magnetic frustration, Rev. Mod. Phys. **85**, 1473 (2013).

[43] A. V. Chumak, V. I. Vasyuchka, A. A. Serga, and B. Hillebrands, Magnon spintronics, Nat. Phys. **11**, 453 (2015).

[44] Jacob Torrejon, Mathieu Riou, Flavio Abreu Araujo, Sumito Tsunegi, Guru Khalsa, Damien Querlioz, Paolo Bortolotti, Vincent Cros, Kay Yakushiji, Akio Fukushima, Hitoshi Kubota, Shinji Yuasa, Mark D. Stiles, and Julie Grollier, Neuromorphic computing with nanoscale spintronic oscillators, Nature **547**, 428 (2017).